# Optical behavior of self-assembled high-density Ge nanoislands embedded in $SiO_2$

**Alireza Samavati[1], Zulkafli Othaman[1], Sib Krishna Ghoshal[2*], and Samad Zare[1]**

[1]*Ibn Sina Institute for Fundamental Science Studies, Universiti Teknologi Malaysia, Skudai, Johor, Malaysia*

[2]*Advanced Optical Material Research Group, Department of Physics, Faculty of Science, Universiti Teknologi Malaysia, 81310 UTM Skudai, Johor, Malaysia*

[*]*Corresponding author: krishnasib@gmail.com*

Received June 21, 2013; accepted September 16, 2013; posted online November 4, 2013

The radio frequency magnetron sputtering method is used to prepare well-dispersed pyramidal-shaped Ge nanoislands embedded in amorphous $SiO_2$ sublayers of various thicknesses. The estimated size and number density of Ge nanoislands in $SiO_2$ sublayer thicknesses beyond 30 nm are approximately 15 nm and $10^{11}$ $cm^{-2}$, respectively. Atomic force microscopy (AFM) reveals root mean square (RMS) roughness sensitivity as the $SiO_2$ sublayer thickness varies from 30 to 40 nm. The formation of nanoislands with high aspect ratios is attributed to the higher rate of surface reactions between Ge adatoms and nucleated Ge islands than reactions associated with $SiO_2$ and Ge. The Ge nanoisland polyorientation on $SiO_2$ (50-nm thickness) is revealed by X-ray diffraction (XRD) patterns. Photoluminescence (PL) peaks of 2.9 and 1.65 eV observed at room temperature (RT) are attributed to the radiative recombination of electrons and holes from the Ge nanoislands/$SiO_2$ and $SiO_2$/Si interfaces, respectively. The mean island sizes are determined by fitting the experimental Raman profile to two models, namely, the phonon confinement model and the size distribution combined with phonon confinement model. The latter model yields the best fit to the experimental data. We confirm that $SiO_2$ matrix thickness variations play a significant role in the formation of Ge nanoislands mediated via the minimization of interfacial and strain energies.

*OCIS codes:* 250.5230, 170.5660.

*doi: 10.3788/COL201311.112502.*

The phenomenon of self-assembly in nanotechnology is of paramount significance in several areas of material processing and fabrication. Understanding the importance of the growth mechanisms and atomic processes that occur on the surface of semiconductor nanostructures in condensed media is challenging. Si and Ge nanostructures, among other types of semiconductors, have received much attention because of their small-sized particles. Such particles help increase the efficiency of optical transitions by several orders of magnitude, thereby allowing the use of the nanostructures in a wide range of nanophotonic applications. Dielectric layers with embedded semiconductor nanocrystals have been widely studied with the aim of overcoming the complexities of non-volatile memory devices with continuous miniaturization, such as Si-based light emitting diodes (LEDs)[1]. Low-dimensional memory devices are unreliable because of their restricted dimensions, which yield issues related to defects in the tunneling layer and lateral charge losses[2]. Such problems may be avoided by embedding semiconductor nanocrystals, such as Ge and Si, into the insulator as charge-storage media[3]. To utilize carrier confinement at room temperature (RT), the sizes of the embedded nanostructures must be comparable with the exciton Bohr radius. While the typical size of self-organized Ge/Si islands is usually much larger than this radius[4,5], the growth of Ge islands on a Si surface covered by a thin layer of $SiO_2$ results in the formation of ultra-small islands[6].

While the formation of self-assembled Ge islands on Si substrates is compressively strained because of the 4% lattice mismatch between Si and Ge, the growth of Ge islands on $SiO_2$ is even more strained and coupled strongly to the substrate surface. This strong strain leaves the Ge islands vulnerable to oxidation, which can reduce strain. Unlike the growth of Ge on pure Si surfaces, Ge nanoisland formation on $SiO_2$ does not follow the S–K growth mode; this finding can be explained by the Volmer–Weber growth mode[7]. In the Volmer–Weber mode, three-dimensional islands are grown on substrate surfaces without the formation of a wetting layer.

Growth by sputtering involves two main competing mechanisms. The first mechanism is the shadowing effect, which leads to preferred growth in the vertical direction. The second mechanism is surface diffusion, which tends to smooth the growing surface. The morphological evolution of the growing surface is driven by competition between these mechanisms. At the initial stage of deposition, growth of a smooth film is possible. The surface remains flat until a critical thickness is reached, after which subsequent growth leads to a roughening transition[8]. In this letter, we report the characterization, growth mechanism, $SiO_2$ thickness-dependent structural evolution, and optical properties of Ge nanoislands/$SiO_2$/Si obtained via the radio frequency (RF) magnetron sputtering technique.

A series of Ge nanoislands were grown on $SiO_2$/Si (100) via the RF magnetron sputtering technique (HVC Penta Vacuum). The samples were grown from polycrystalline $SiO_2$ and Ge targets (99.999% purity) on Si (100) p-type wafers at a substrate temperature of 400 °C. Initially, a $SiO_2$ layer was deposited at three different times of 40, 60, and 90 min to achieve 30-nm (sample A), 40-nm (sample B), and 50-nm (sample C) thicknesses, respectively.

 © 2013 Chinese Optics Letters

Ge was then sputtered onto the wafer for 420 s under similar conditions. After the deposition of each layer, the plasma was turned off and the chamber was evacuated until a pressure of around $2\times10^{-5}$ Torr was achieved. The total working pressure in the chamber was kept constant at $2\times10^{-3}$ Torr during deposition. The RF powers applied on the $SiO_2$ and Ge targets were 250 and 100 W, respectively, and the Ar flow rate was kept constant at 10 sccm. The samples were kept inside the chamber to cool to RT after growth. The structural details of the samples were studied by X-ray diffraction (XRD) (D8 Advance Diffractometer, Bruker, USA ) using Cu-K$\alpha$ radiation (0.154 nm) at 40 kV and 100 mA. The $2\theta$ range was set to 0°–90° with a step size of 0.02° and a resolution of 0.011°. Photoluminescence (PL) spectra were recorded at RT using a luminescence spectrometer (LS 55, Perkin Elmer, USA) under 259-nm excitation. Raman spectroscopy was performed using a Spectrum GX (Near infrared Fourier transform (NIR-FT) Raman) system with a Nd crystal laser source featuring a 1-$\mu$m spot size with 50-m W laser power.

Figure 1 represents atomic force microscopy (AFM) images the self-assembled nanoislands grown on $SiO_2$ sublayers with varying thicknesses and an area of 1 ×1 ($\mu$m). The corresponding size distributions and nanoisland shapes are shown as insets. The surface of sample A is inhomogeneous and smooth with low nanoisland density. Inhomogeneity and smoothness are attributed to a lack of nucleation and nanoisland growth, both of which are effects of high interfacial and strain energies. The formation of Ge nanoislands becomes more prominent with increases in the height and length of pyramidal shaped islands as the thickness of the $SiO_2$ sub-layer increases from 30 to 50 nm. Enhanced nanoisland formation is attributed to enhanced diffusion and Ge atoms nucleation at the matrix surface, both of which lead to ordering and lowered free energies.

The formation of pyramidal-shaped islands is attributed to the significantly higher rate of surface reactions between Ge adatoms and nucleated Ge islands during Ge deposition in comparison with reactions between Ge adatoms and $SiO_2$. This mechanism causes hindrances during the formation of a wetting Ge layer on the $SiO_2$ surface and brings about higher aspect ratios (height divided by base length, ∼0.33) of the Ge islands. By contrast, the formation of a wetting Ge layer on the Si substrate is favorable; this mechanism causes enhanced reaction rates between Ge adatoms and the substrate, which is reported to yield a lower aspect ratio for Ge islands[9,10]. The present study reveals that the growth of high-density Ge nanoislands on $SiO_2$ is more favorable than the growth of nanoislands on Si substrates for optoelectronic applications, which is in good agreement with findings by Kolobov *et al.*[11].

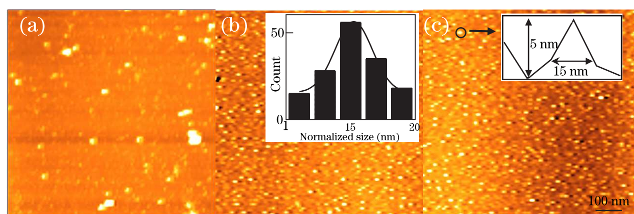


Fig. 1. (Color online) Two-dimensional AFM images of Ge nanoislands on $SiO_2$ sublayers with thicknesses of (a) 30, (b) 40, and (c) 50 nm. Inset: (b) size distribution; (c) pyramidal-shaped structure.

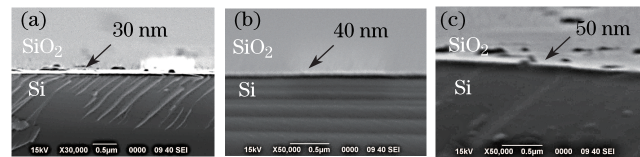


Fig. 2. SEM images of cross-sections obtained during the formation of different $SiO_2$ sublayer thicknesses.

**Table 1. RMS Roughness, Number Density, and Grain Area Ratio as a Function of $SiO_2$ Thickness**

| Sample | $SiO_2$ Thickness (nm) | RMS Roughness (nm) | Number Density ($cm^{-2}$) | Ratio of Grain Area |
|---|---|---|---|---|
| A | $30 \pm 1$ | $0.12 \pm 0.03$ | $\sim 2.1 \times 10^9$ | 15% |
| B | $40 \pm 1$ | $0.56 \pm 0.02$ | $\sim 5.1 \times 10^{11}$ | 30% |
| C | $50 \pm 2$ | $0.61 \pm 0.02$ | $\sim 5.8 \times 10^{11}$ | 28% |

Scanning electron microscopy (SEM) micrographs of the cross-sections of the nanoislands on the Si substrate are shown in Fig. 2; these images confirm the presence of $SiO_2$ sublayers with thicknesses of 30, 40, and 50 nm on the Si substrate. The $SiO_2$ sublayer-thickness-dependent root mean square (RMS) roughness of the Ge nanoislands is illustrated in Table 1. The RMS roughness of the surface continuously increases as the thickness of the sublayer increases from 30 to 50 nm. However, the surface roughness, the grain area ratio, and the number density are relatively insensitive to $SiO_2$ thickness variations from 40 to 50 nm. This result is a consequence of adatom attachment to the nucleated islands, which dominates over individual adatom nucleation.

Figure 3 illustrates the energy dispersive X-ray (EDX) spectra of samples A and C. The Ge layer begins to form island structures when the $SiO_2$ sublayer thickness increases from 30 to 50 nm. At 30-nm thickness, the surface is mainly smooth with minimal Ge island density. However, by increasing the $SiO_2$ thickness to 50 nm, the island density increases by several orders of magnitude, which results in an effective decrement of the Ge content. High Si contents originate from the substrate. Au and C peaks observed in the spectra are attributed to the fine conductive coating used, the glue used to hold the samples for recording EDX spectra, and the simultaneous performance of field emission scanning electron microscopy (FESEM) and EDX. The recorded FESEM images (not shown here) confirm the presence of Ge nanoisland sizes ranging from 15 to 20 nm, which is in agreement with the XRD and AFM results.

The XRD spectra of samples A and C are presented in Fig. 4. Sample C clearly shows Ge crystallization on the $SiO_2$ sublayer with a thickness of 50 nm. This sample further exhibits a polyoriented structure with several characteristic peaks corresponding to other crystalline planes, such as (111), (004), (220), and (311). The peak at 57° can be assigned to reflections from the (012) plane with a hexagonal symmetry relative to the

$GeO_2$ nanocrystalline phase[12]. The peak corresponding to the amorphous $SiO_2$ sublayer structure appears at lower angles of 20°–30° and has a full width at half maximum (FWHM) of approximately 4°[13].

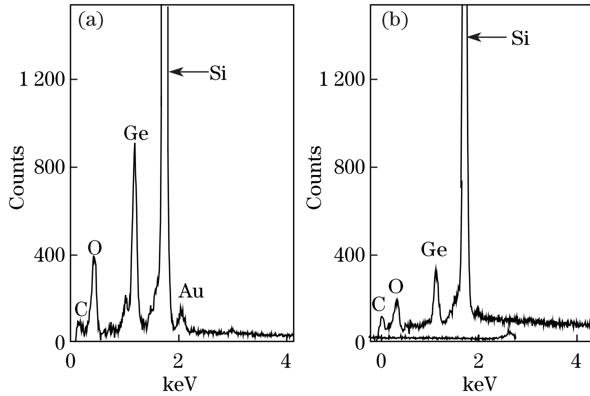


Fig. 3. (color online) EDX spectra of samples (a) A and (b) C.

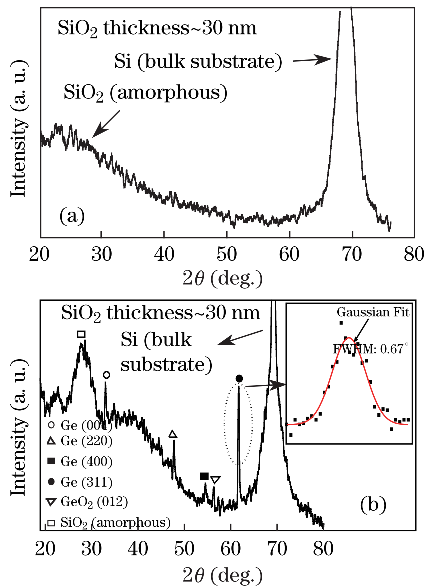


Fig. 4. XRD pattern of Ge nanoislands deposited on $SiO_2$ sublayers with thicknesses of (a) 30 and (b) 50 nm. Gaussian fitted of intense Ge peak at (311) orientation plane.

At $SiO_2$ sub-layer thicknesses of ~30 nm and below, the growth of $Ge/SiO_2/Si$ proceeds layer-by-layer with strain relaxation mediated by misfit dislocation nucleation rather than island formation. By contrast, at sublayer thicknesses above 30 nm, the growth mechanism of crystals follows the Volmer–Weber mode. Interestingly, the Ge nanoislands embedded in the 50-nm $SiO_2$ matrix display more complex defect structures than the nanoislands embedded in matrices of other thicknesses. This phenomenon is attributed to the presence of misfit dislocations and very small pyramidal stacking faults at the Ge/Si interface as well as threading dislocations propagating across the Ge thickness. Pronounced surface roughening observed on $SiO_2$ sublayers with thicknesses above 30 nm originates from various types of dislocations and stacking faults. The (311) peak may be used to estimate the mean nanoisland size via Scherrer's formula: $D = 0.9\lambda/\beta\cos\theta$, where $D$ is the average crystalline size, $\lambda$ is the X-ray wavelength (0.15418 nm), $\beta$ is the angular line width of half-maximum intensity, and $\theta$ is Bragg's angle expressed in degrees[14]. The average size of the Ge nanoislands is estimated to be ~13 nm, which agrees with the AFM and Raman data.

The RT PL spectra shown in Fig. 5 exhibit a strong peak centered at 2.9 eV regardless of the thickness of the $SiO_2$ sub-layer. The origin of visible luminescence is attributed to the radiative recombination of electrons and holes in the quantum-confined nanostructures, which can be explained using the Ge nanoislands/$SiO_2$/Si interface model depicted in Fig. 6. Some researchers have argued that if the potential well that confines electrons in the conduction band has sufficient depth, the corresponding radiative recombination would involve holes and electrons confined within the Ge nanoislands. The energy required for radiative recombination is approximately from 2 to 3 eV. The potential barrier at the Ge nanoislands/$SiO_2$ interface can only confine electrons with energies of approximately 1.5–2 eV above the conduction band edge. Therefore, electron states with such high energies can only exist as structural defects in $SiO_2$ sublayer. This finding suggests that radiative recombination involves no electrons from the conduction band of the Ge or Si; instead, electrons that are localized in the radiative defect states at the Ge nanoislands/$SiO_2$ interfaces participate in recombination. A similar description for Ge nanocrystals embedded in a $SiO_2$ matrix has been suggested by Takeoka *et al.*[15].

The excitation energy-dependent PL spectra suggest the active role of defects because electron states with defects typically have broader energy distributions[16,17]. Therefore, lower energy states can be involved through relatively lower excitation energies of the laser beams than the higher one reported earlier[18]. The Ge nanoisland structures in the present study contain a boundary between the Si substrate and the $SiO_2$ sublayer, which is responsible for the observed weak PL peak of approximately 1.65 eV. Nishikawa *et al.*[19] also observed that a PL peak from 1.5 to 1.7 eV originated from $SiO_2$/Si interfaces. The weak peak found in this study is attributed to radiative recombination at the Si/$SiO_2$ interface, which is much weaker than that at the Ge nanoislands/$SiO_2$ interface (Fig. 5, inset).

The Raman spectra of the nanoislands, which can be used to identify various species and their crystal phases, are recorded and presented in Fig. 7. Raman spectra contain information on the vibrations (phonon modes) of entire molecules or crystals. Phonons have important influences on the physical, structural, and optical properties of many crystals. The effect of confinement in

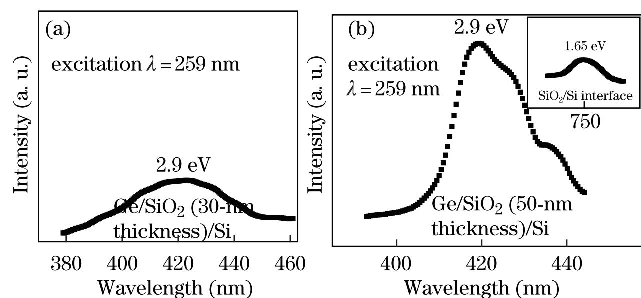

Fig. 5. PL spectra of Ge nanoislands embedded on $SiO_2$ sublayers with thicknesses of (a) 30 and (b) 50 nm. Inset in (b): $SiO_2$/Si interface reaction peak.

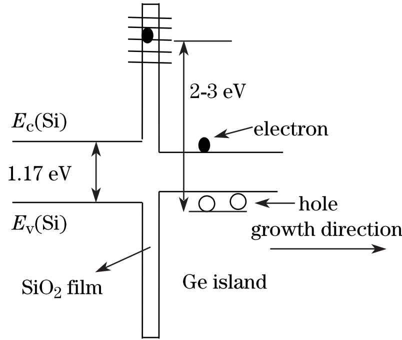


Fig. 6. Schematic band structure of Ge nanoislands/$SiO_2$/Si. Dotted lines indicate energy levels in the Ge islands and $SiO_2$ sublayer. The energy of 1.17 eV corresponds to the bulk Si band gap.

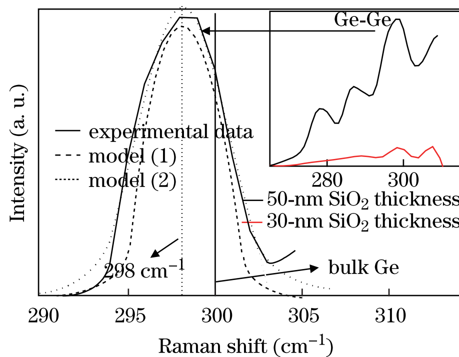


Fig. 7. (Color online) Raman spectra around the Ge peak with Gaussian-fitted spectrum. Inset: raw data.

low dimensional systems, in general, and nanocrystalline systems, in particular, can restrict some phonons or vibrational modes. This restriction, also called quantization, is manifested in different behaviors, such as vibrations that shift toward different energies, changes in the symmetry of the vibration peaks, and variations in peak intensity.

The Raman spectrum of sample C (inset in Fig. 7) consists of three bands located at around 278, 289, and 298 $cm^{-1}$. The band at around 298 $cm^{-1}$ is assigned to the first-order transverse optical phonon mode of the Ge nanoislands, which is in agreement with the results of Kartopu *et al.*[20]. The strongest Raman peak (i.e., 298 $cm^{-1}$), which corresponds to the Ge–Ge phonon mode, shows a shift towards lower frequencies with respect to the Raman peak of bulk crystalline Ge (i.e., approximately 300 $cm^{-1}$). Asymmetric bands that appear between 260 and 290 $cm^{-1}$ are attributed to the Ge–O phonon mode, which is consistent with the report of Giri *et al.*[21].

The peak at 298 $cm^{-1}$ exhibits two interesting features. Firstly, the spectrum possess a well-defined peak with a characteristic shape that is essentially identical to that of bulk Ge crystals reported by Kartopu *et al.* The presence of this band in our spectrum confirms the existence of Ge nanoislands in the $SiO_2$ sublayer. Secondly, the spectrum is wider, slightly asymmetrical, and red-shifted compared with that of bulk Ge. According to Wellner *et al.*[22], displacements in the position of the Raman peak of Ge nanostructures with respect to that of bulk Ge are caused by isotopic effects, phonon confinement, and stress effects from the $SiO_2$ sublayer on the Ge nanostructures.

Following the work of Fauchet *et al.*[23], the Raman spectra of sample C was fitted to a theoretical model to examine the effect of nanocrystal size distribution on the spectral line shape. According to this model, the first-order Raman spectrum, $I(w)$, as a function of frequency $(w)$ is given by

$$I(w) = \int \frac{4\pi q^2 |C(0,q)|^2}{[w - w(q)]^2 + \left[\frac{\Gamma_c}{2}\right]^2} \mathrm{d}q, \tag{1}$$

where $w(q)$ is the phonon dispersion curve, vector $\boldsymbol{q}$ is expressed in $2\pi/a$ units, $a$ is the Ge lattice constant (0.566 nm), $L$ is the Ge nanocrystallite diameter, and $\Gamma_c$ is the natural line width for crystalline Ge at RT (3 $cm^{-1}$). By comparing the calculated Raman spectra with the experimental results, the Gaussian confinement function is found to be the most suitable for semiconductor microcrystallites[23]. Therefore, $w(r, L)$ is expressed as

$$w(r, L) = \exp\left(\frac{-8\,\pi^2\, r^2}{L^2}\right),$$

$$|C(0, q)|^2 = \exp\left(\frac{-q^2\, L^2}{16\pi}\right).$$

The size distribution profile obtained from the AFM micrographs is used together with Eq. (1) to yield:

$$I(w) = \int \rho\,(L)\mathrm{d}L \times \int \frac{4\pi\, q^2\, |C(0,q)|^2}{[w - w\,(q)]^2 + \left[\frac{\Gamma_c}{2}\right]^2} \mathrm{d}q, \tag{2}$$

where $\rho(L)$ is the size distribution of the sample. The model in Eq. (2) was previously used by Hernandez *et al.*[24,25].

The experimental Raman spectra in Fig. 6 (upper solid curve) were used to fit the models in Eqs. (1) (lower dashed curve) and (2) (middle dotted curve) by adjusting the $L$ value (assuming spherical shaped nanocrystals), and the best fit was obtained. The dashed line observed for crystals with single sizes deviates significantly from the experimental curve, while the dotted line generated using the Gaussian distribution matches the experimental curve well. Furthermore, size variations in the nanocrystals are unable to produce measurable blue shifts in the Raman spectra. The estimated sizes of the Ge nanocrystallites obtained using Eqs. (1) and (2) are approximately 10 and 12 nm, respectively. Fujii *et al.*[26] suggested that disagreements between the theoretical and experimental Raman peak frequencies may be caused by the stress exerted on the Ge nanocrystals.

In conclusion, high-density Ge nanoislands embedded in various $SiO_2$ sublayer thicknesses are prepared using RF magnetron sputtering. The formation of Ge nanoislands and their optical behaviors are examined by AFM, XRD, EDX, PL, and Raman spectroscopy. AFM results of sample C are further used to determine the size distribution of the nanoisland. The average size of Ge

nanoislands in samples B and C is approximately 15 nm. The strong PL peak at 2.9 eV is attributed to the radiative recombination of electrons and holes from Ge nanoislands/$SiO_2$ interfaces. The experimental Raman spectra are fitted to two models with single and Gaussian size distributions of the nanoislands. The model based on size distribution fits the experimental observations better than the model based on phonon confinement. This disagreement may be caused by the effect of compressive stresses exerted by the $SiO_2$ network on the Ge nanoislands. We establish that embedding Ge on a $SiO_2$ matrix exerts a strong influence on the growth mechanism of the resultant nanostructures mediated by interfacial and strain energies. Our facile sample preparation method and detailed characterization results contribute to future studies on the low-cost fabrication of Ge nanoislands with high density.

This work was supported by visiting researcher grants provided by the MoHE (Nos. Q. J090000. 21A4. 00D20 and Q. J130000. 2526. 02H94).

## References

1. Z. Dong, W. Wang, B. Huang, X. Zhang, N. Guan, and H. Chen, Chin. Opt. Lett. **9,** 082301 (2011).
2. P. Cappelletti, Microelectron. Reliab. **38,** 185 (1998).
3. C. L. Heng and T. G. Finstad, Phys. E **26,** 386 (2005).
4. P. Schnittenhelm, M. Gail, J. Brunner, J. F. Nutzel, and G. Abstreiter, Appl. Phys. Lett. **67,** 1292 (1995).
5. S. A. Chaparro, Y. Zhang, and J. Drucker, Appl. Phys. Lett. **76,** 3534 (2000).
6. A. A. Shklyaev, M. Shibata, and M. Ichikawa, Phys. Rev. B **62,** 1540 (2000).
7. A. I. Nikiforov, V. V. Ulyanov, O. P. Pchelyakov, S. A. Teys, and A. K. Gutakovsky, Mat. Sci. Semicon. Proc. **8,** 47 (2005).
8. R. P. U. Karunasiri, R. Bruinsma, and J. Rudnick, Phys. Rev. Lett. **62,** 788 (1989).
9. J. L. Liu, J. Wan, Z. M. Jiang, A. Khitun, and K. L. Wang, J. Appl. Phys **92,** 6804 (2002).
10. A. R. Samavati, Z. Othaman, S. K. Ghoshal, M. R. Dousti, and R. J. Amjad, Chin. Phys. Lett. **29,** 118101 (2012).
11. A. V. Kolobov, A. A. Shklyaev, H. Oyanagi, P. Fons, S. Yamasaki, and M. Ichikawa, Appl. Phys. Lett. **78,** 2563 (2001).
12. C. Jing, J. Hou, and X. Xu, Opt. Mater. **30,** 857 (2008).
13. Y. Wang, X. Peng, J. Shi, X. Tang, J. Jiang, and W. Liu, Nanoscale Res. Lett. **7,** 86 (2012).
14. J. Giri, S. Thakurta, J. Bellare, A. K. Nigam, and D. Bahadur, J. Magn. Magn. Mater. **293,** 62 (2005).
15. S. Takeoka, M. Fujii, S. Hayashi, and K. Yamamoto, Phys. Rev. B **58,** 7921 (1998).
16. D. D. Chambliss and K. E. Johnson, Phys. Rev. B **50,** 5012 (1994).
17. M. Zinke-Allmang, Thin Solid Films **346,** 1 (1999).
18. A. R. Samavati, Z. Othaman, S. K. Ghoshal, M. Dousti, and M. R. Kadir, Int. J. Mol. Sci. **13,** 12880 (2012).
19. H. Nishikawa, J. H. Stathis, and E. Cartier, Appl. Phys. Lett. **75,** 1219 (1999).
20. G. Kartopu, V. A. Karavanskii, U. Serincan, R. Turan, R. E. Hummel, Y. Ekinci, A. Gunnaes, and T. G. Finstad, Phys. Stat. Sol. A **202,** 1472 (2005).
21. P. K. Giri and S. Dhara, J. Nanomaterials **2012,** 1 (2011).
22. A. Wellner, V. Paillard, C. Bonafos, H. Coffin, A. Claverie, B. Schmidt, and K. H. Heining, J. Appl. Phys. **94,** 5639 (2003).
23. P. M. Fauchett and I. H. Campbell, Crit. Rev. Solid State Mater. **14,** S14 (1988).
24. J. G. Hernandez, G. H. Azarbayejani, R. Tsu, and F. H. Pollak, Appl. Phys. Lett. **47,** 1350 (1985).
25. C. E. Bottani, C. Mantini, P. Milani, M. Manfredini, A. Stella, P. Tognini, P. Cheyssac, and R. Kofman, Appl. Phys. Lett. **69,** 2409 (1996).
26. M. Fujii, S. Hayashi, and K. Yamamoto, Jpn. J. Appl. Phys. **30,** 687 (1991).